Acta Chemica Scandinavica A 33 (1979) 469–480

Compounds with the Marcasite Type Crystal Structure. XIII. Structural and Magnetic Properties of $Cr_tFe_{1-t}As_2$, $Cr_tFe_{1-t}Sb_2$, $Fe_{1-t}Ni_tAs_2$ and $Fe_{1-t}Ni_tSb_2$

ARNE KJEKSHUS,[a] PER G. PETERZÉNS,[a] TROND RAKKE[a] and ARNE F. ANDRESEN[b]

[a] Kjemisk Institutt, Universitetet i Oslo, Blindern, Oslo 3, Norway and [b] Institutt for Atomenergi, Kjeller, Norway

The structural and magnetic properties of $Cr_tFe_{1-t}As_2$, $Cr_tFe_{1-t}Sb_2$, $Fe_{1-t}Ni_tAs_2$ and $Fe_{1-t}Ni_tSb_2$ have been investigated by X-ray and neutron diffraction and magnetic susceptibility measurements. The structures of the ternary, random solid solution phases are of the FeS_2-*m* type. The antiferromagnetic mode of $CrSb_2$ extends into the ternary region (to $t \approx 0.5$) of $Cr_tFe_{1-t}Sb_2$. No evidence of cooperative magnetism was found for $Cr_tFe_{1-t}As_2$, $Fe_{1-t}Ni_tAs_2$ and $Fe_{1-t}Ni_tSb_2$.

From the existence, structure and magnetic properties of the compound $CrSb_2$,[1] three natural questions arise:

(i) Why are the corresponding compounds CrP_2, $CrAs_2$ and $CrBi_2$ not obtained[2,3] by the application of similar preparative conditions (*viz.* not involving high pressure)?

(ii) Why does $CrSb_2$ take the FeS_2-*m* type structure? (Under the more extreme conditions of high pressure-high temperature, compounds with formulae CrP_2 and $CrAs_2$ are obtained,[4] but with the $NbAs_2$ type rather than the $FeSe_2$-*m* type structure.)

(iii) Why is $CrSb_2$ the only FeS_2-*m* type compound which exhibits cooperative magnetic behaviour?

In order to shed some light on question (i), part of this study has been concerned with the properties of the hypothetical FeS_2-*m* type compound $CrAs_2$. Another aim has been to gain more insight into the cooperative magnetic properties of $CrSb_2$ [question (iii)] through examination of $Cr_tFe_{1-t}Sb_2$.

The family of FeS_2-*m* type compounds are conveniently divided into two distinct classes A and B, and a transitional class A/B (*cf.* Ref. 5 and references therein). The phases $Cr_tFe_{1-t}As_2$ and $Cr_tFe_{1-t}Sb_2$ belong to the same class (A), and in order to give the structural part of this study a somewhat wider scope, selected samples from the class A/B type $Fe_{1-t}Ni_tAs_2$ and $Fe_{1-t}Ni_tSb_2$ phases have also been included. (Structural details of the binary compounds $CrSb_2$, $FeAs_2$, $FeSb_2$, $NiAs_2$ and $NiSb_2$ are already at hand.[1,6,7]) We have earlier published[2] ^{57}Fe Mössbauer spectroscopic data for $Cr_tFe_{1-t}As_2$, $Cr_tFe_{1-t}Sb_2$, $Fe_{1-t}Ni_tAs_2$ and $Fe_{1-t}Ni_tSb_2$. Some phase analytical data for these phases are included in Refs. 2, 5, 8 and 9.

EXPERIMENTAL

The pure elements used as starting materials for the syntheses were 99.999 % Cr-flakes (Koch-Light Laboratories), turnings from 99.99+ % Fe- and 99.995 % Ni-rods (Johnson, Matthey & Co.), 99.9999 % As and 99.9995 % Sb (Koch-Light Laboratories). According to earlier experience[2,8,9] with syntheses of ternary phases, equilibria are most readily attained when preparations of the binary compounds are introduced as intermediate steps in the procedures.

$FeAs_2$ and $NiAs_2$ (*viz.* β-$NiAs_2$) were made as described in Ref. 6, $FeSb_2$ and $NiSb_2$ according to the procedure in Ref. 5. The latter scheme has also been adopted successfully here in the preparation of $CrSb_2$. (Thus, the initial synthesis of CrSb has also for $CrSb_2$ virtually eliminated the rather time-consuming grinding and annealing cycles earlier reported.[10]) The final preparational steps for

0302-4377/79/060469-12$02.50
© 1979 Acta Chemica Scandinavica

$Cr_tFe_{1-t}Sb_2$, $Fe_{1-t}Ni_tAs_2$ and $Fe_{1-t}Ni_tSb_2$ are described in Refs. 2 and 5.

A number of small scale (~2 g) $Cr_tFe_{1-t}As_2$ samples (for phase analytical and magnetic susceptibility measurements) and selected larger scale samples (for neutron diffraction studies) were synthesized according to the procedure in Ref. 2.

All samples were examined by powder X-ray (Guinier) diffraction ($CuK\alpha_1$ radiation, $\lambda = 1.54050$ Å) and unit cell dimensions derived by applying the method of least squares (KCl as internal standard, $a = 6.2919$ Å). The small scale $Cr_tFe_{1-t}As_2$ samples were also examined by metallographic methods to ensure homogeneity, and their magnetic susceptibilities measured on 40 to 60 mg samples between 90 and 950 K by the Faraday method (max. field ~8 kOe).

Single crystals of $CrSb_2$ were made for magnetic susceptibility measurements by chemical transport reactions in evacuated and sealed silica capsules. Cr-flakes, Sb-lumps and a few, small crystals of anhydrous $CrCl_3$ (acting as the transport agent) were placed in the hot end (~700 °C). The $CrSb_2$ crystals grew in a zone between 580 and 620 °C, the largest and most perfect crystals being found at the lowest temperature. Surprisingly, a few dark-coloured single crystals of Cr_2O_3 were found in the hot zone. The problem of Cr_2O_3 contamination was also observed in the $Cr_tFe_{1-t}Sb_2$ series. During the syntheses of $Cr_tFe_{1-t}As_2$ (as well as in earlier attempts[2] to prepare $CrAs_2$) this contamination was, on the other hand, not detected.

The powder neutron diffraction data were collected between 10 K and room temperature (operating a DISPLEX cooling system) using cylindrical sample holders of vanadium. Neutrons of wavelength 1.877 Å were obtained from the Kjeller reactor JEEP II. The nuclear scattering lengths $b_{Cr} = 0.353$, $b_{Fe} = 0.951$, $b_{Ni} = 1.03$, $b_{As} = 0.64$ and $b_{Sb} = 0.564$ (in 10^{-12} cm) were taken from Ref. 11. The profile refinement programme of Rietveld[12] was applied in the final fitting of the variable parameters.

RESULTS AND DISCUSSION

(i) Phase analytical data. All the phases $Cr_tFe_{1-t}As_2$, $Cr_tFe_{1-t}Sb_2$, $Fe_{1-t}Ni_tAs_2$ and $Fe_{1-t}Ni_tSb_2$ have earlier been subjected to some phase analytical investigations.[2,5,8,9] However, the $Cr_tFe_{1-t}As_2$ phase has hitherto only been examined rather superficially,[2,13] particularly with respect to its Cr rich phase boundary.

The (orthorhombic) unit cell dimensions of $Cr_tFe_{1-t}As_2$ as determined from samples quenched from 600 °C are shown in Fig. 1. According to

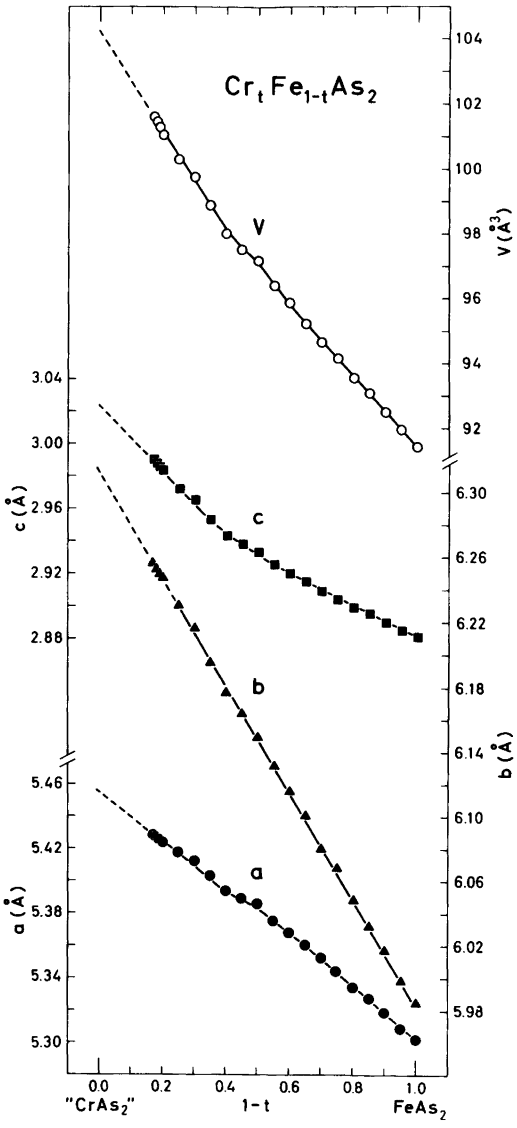

Fig. 1. Room temperature unit cell dimensions *versus* composition for $Cr_tFe_{1-t}As_2$ samples quenched from 600 °C.

X-ray and metallographic evidences, the solid solubility of $Cr_tFe_{1-t}As_2$ extends from $t = 0$ to $t = 0.83 \pm 0.01$ in samples quenched from 600 °C. Supplementary data on samples quenched from temperatures between 600 and 850 °C indicate that the Cr rich phase boundary is shifted only slightly, becoming $t = 0.81 \pm 0.01$ at 850 °C.

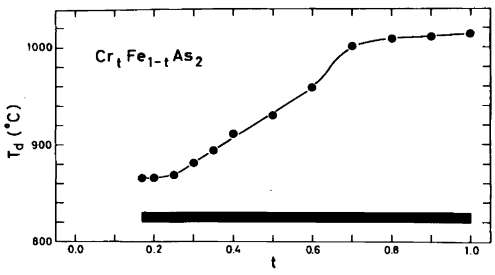

Fig. 2. Decomposition temperature (T_d) for $Cr_tFe_{1-t}As_2$ as a function of (nominal) t.

Decomposition reactions (as determined from DTA, quenching and high temperature X-ray experiments) according to $Cr_tFe_{1-t}As_2 \rightarrow Cr_tFe_{1-t}As + As$, take place between 865 ± 5 °C for $t = 0.80$ and 1014 ± 7 °C for $t = 0$, the variation of decomposition temperature with (nominal, *vide supra*) t being shown in Fig. 2. Thus, the composition corresponding to $t = 0.83 \pm 0.01$ must be the most Cr rich sample that can be obtained at temperatures above 600 °C. On account of these findings, preparational procedures involving temperatures lower than 600 °C are the only contingency worth looking into to conjure forth more Cr rich $Cr_tFe_{1-t}As_2$ samples. This sheds some light on earlier unsuccessful attempts to prepare $CrAs_2$.[2,14]

The possibility that one or more of the phases $Cr_tFe_{1-t}As_2$, $Cr_tFe_{1-t}Sb_2$, $Fe_{1-t}Ni_tAs_2$ and $Fe_{1-t}Ni_tSb_2$ take a metal to non-metal atomic ratio significantly different from 1:2 (depending on temperature and/or the compositional parameter t) has not been systematically studied. However, scattered attempts to test how the matter stands have invariably demonstrated the 1:2 composition. It is worth noting that the free antimony often observed during annealing of $Cr_tFe_{1-t}Sb_2$, originates from partial oxidation of the samples (*cf.* Experimental) rather than providing evidence for a deviation (see Refs. 15 and 16 for $CrSb_2$) from the 1:2 composition.

(ii) Structural data. Structural data for various compositions of the phases under investigation are given in Table 1. The unit cell dimensions (shown graphically in Fig. 3 to demonstrate consistency with earlier findings) were obtained from Guinier photographic data, whereas all positional parameters were derived by profile refinement of powder neutron diffraction recordings. A description of the FeS_2-*m* type structure in terms of space group *Pnnm* has been assumed in all calculations (*cf.* Refs. 6, 17 and 18).

Since the room temperature values of the positional parameters, $x = 0.1797(2)$ and $y = 0.3662(2)$, given in Ref. 1 for $CrSb_2$ clearly broke the pattern of $Cr_tFe_{1-t}Sb_2$ (Fig. 4), $CrSb_2$ was reexamined.

Table 1. Structural data for $Cr_tFe_{1-t}As_2$, $Fe_{1-t}Ni_tAs_2$, $Cr_tFe_{1-t}Sb_2$ and $Fe_{1-t}Ni_tSb_2$ at room temperature.

Phase	t	a(Å)	b(Å)	c(Å)	x	y
$Cr_tFe_{1-t}As_2$	0.79	5.4174(6)	6.2433(6)	2.9803(4)	0.1692(4)	0.3702(3)
	0.63	5.3971(11)	6.1893(18)	2.9539(10)	0.1706(4)	0.3681(4)
	0.47	5.3771(11)	6.1368(17)	2.9309(9)	0.1723(5)	0.3667(3)
	0.32	5.3544(13)	6.0853(15)	2.9112(7)	0.1730(6)	0.3649(4)
	0.00	5.3013(7)	5.9859(5)	2.8822(3)	0.1763(10)	0.3624(7)
$Fe_{1-t}Ni_tAs_2$	0.25	5.2309(9)	5.9555(11)	2.9693(9)	0.1786(7)	0.3641(4)
	0.50	5.1377(7)	5.9205(5)	3.1077(4)	0.1850(6)	0.3662(5)
	1.00	4.7583(7)	5.7954(7)	3.5449(4)	0.2017(8)	0.3691(7)
$Cr_tFe_{1-t}Sb_2$	1.00	6.0275(6)	6.8738(9)	3.2715(7)	0.1764(7)	0.3638(6)
	0.93	6.0205(15)	6.8491(13)	3.2628(9)	0.1772(7)	0.3634(5)
	0.88	6.0156(10)	6.8341(10)	3.2569(5)	0.1779(5)	0.3624(4)
	0.72	5.9862(12)	6.7810(10)	3.2370(8)	0.1797(5)	0.3613(4)
	0.60	5.9632(12)	6.7391(11)	3.2233(6)	0.1812(6)	0.3604(5)
	0.45	5.9378(7)	6.6886(7)	3.2147(4)	0.1830(5)	0.3601(4)
	0.21	5.8833(17)	6.6072(20)	3.2004(12)	0.1865(6)	0.3579(5)
	0.00	5.8328(5)	6.7356(5)	3.1973(3)	0.1885(2)	0.3561(4)
$Fe_{1-t}Ni_tSb_2$	0.25	5.7535(11)	6.4928(10)	3.2681(7)	0.1929(7)	0.3571(6)
	0.50	5.6417(9)	6.4402(9)	3.3855(5)	0.1964(7)	0.3597(6)
	1.00	5.1837(6)	6.3184(10)	3.8408(6)	0.2189(10)	0.3593(8)

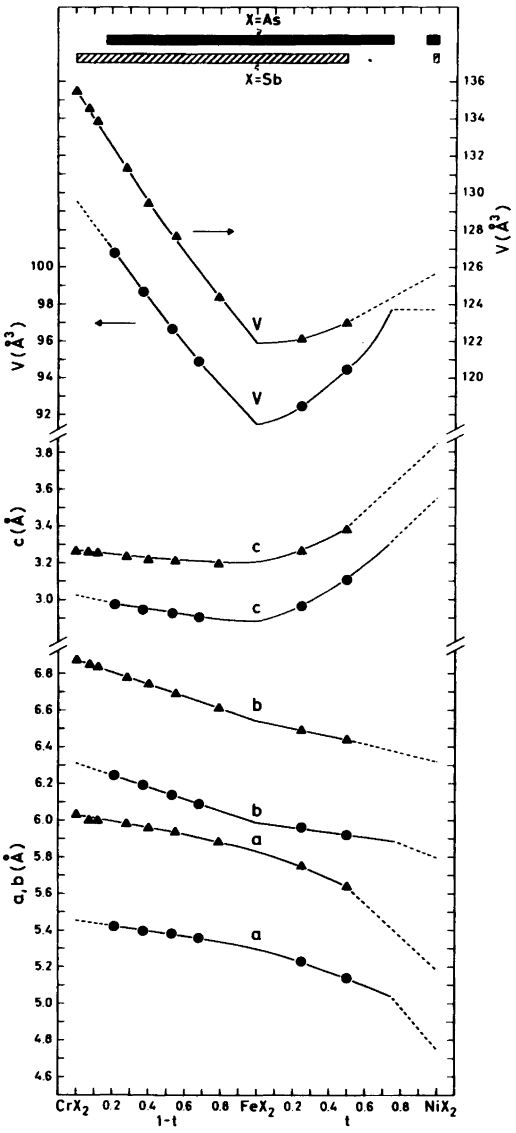

Fig. 3. Room temperature unit cell dimensions for the samples investigated by neutron diffraction. Fully traced curves represent least square fits to data given in Refs. 2, 8, 9 and Fig. 1. Symbols ● and ▲ refer to $X = As$ and $X = Sb$, respectively.

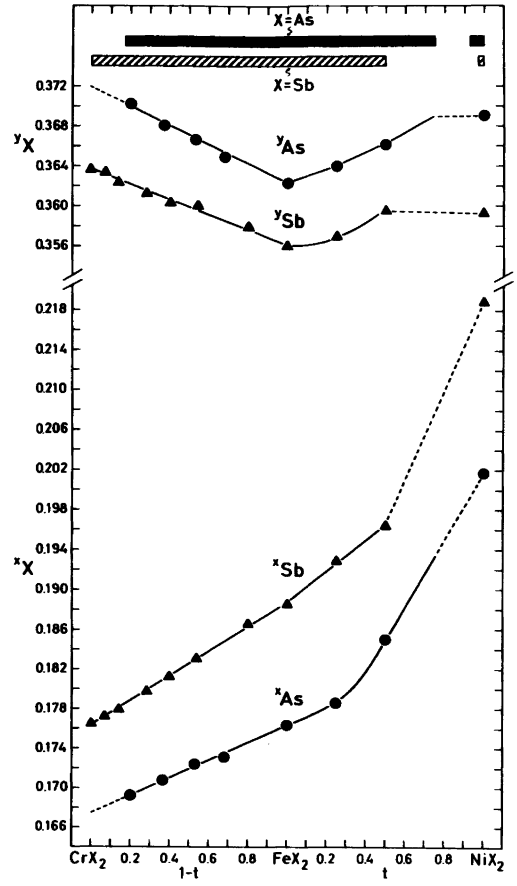

Fig. 4. Positional parameters (at room temperature, but temperature variations are minor, almost insignificant) *versus* composition for $Cr_tFe_{1-t}X_2$ and $Fe_{1-t}Ni_tX_2$.

As seen from Fig. 4, the redetermined values (Table 1) remedied the discrepancy.

As an additional check on sample compositions, occupation-number parameters were allowed to vary during the initial neutron diffraction profile refinement cycles. This sort of correction procedure proved to be significant (as the Guinier photographic data had already brought out) only for the $Cr_tFe_{1-t}Sb_2$ samples (due to partial oxidation, see section *i*). The corrected compositions for the $Cr_tFe_{1-t}Sb_2$ samples as obtained from occupation-number on the one hand, and previously known unit cell dimensions on the other, were in excellent mutual agreement (max. deviation in $t < 0.02$).

The initial data for some of the $Cr_tFe_{1-t}As_2$ samples proved impossible to refine to acceptable values of the *R* factor without including a preferred orientation parameter. After such corrections, refinements converged to *R* factors ≤ 0.045. Duplicated data sets were also collected for these samples and

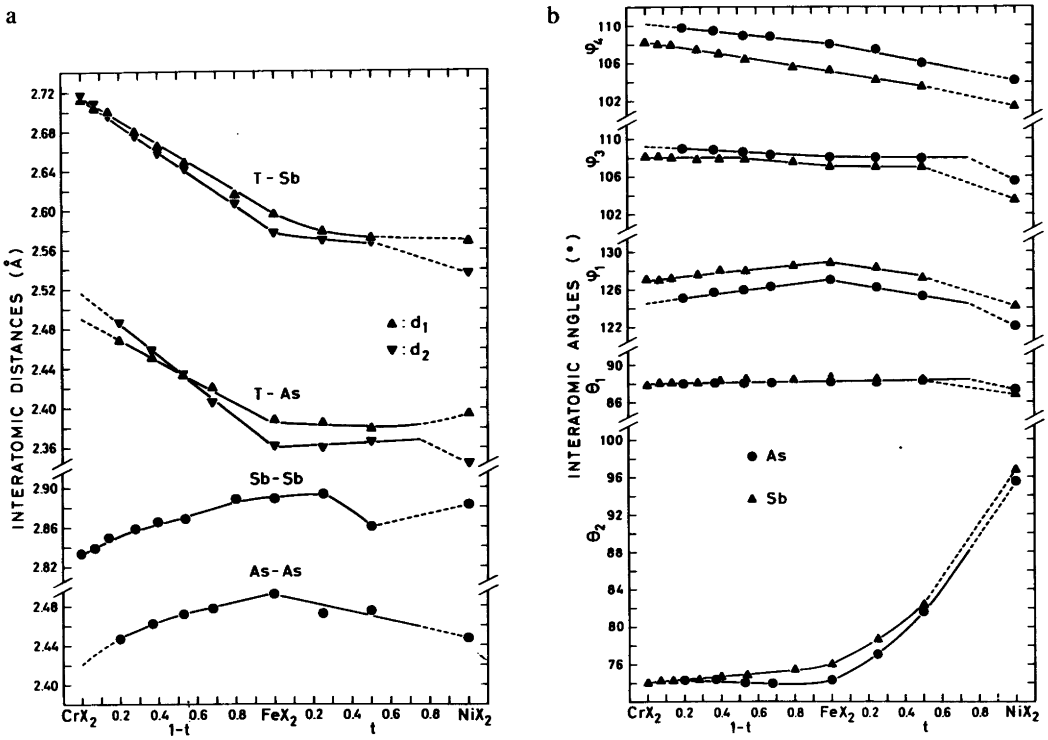

Fig. 5. Interatomic distances (a) and angles (b) at room temperature as a function of composition for $Cr_tFe_{1-t}X_2$ and $Fe_{1-t}Ni_tX_2$.

by paying particular attention when loading the specimens into the sample holder, the preferred orientation correction turned out to be virtually unimportant. However, microscopic examination of these samples did not reveal shapes consistent with the assumption of preferred orientation.

On the basis of the data in Table 1 (Ref. 6 for NiX_2) and in terms of notations defined in Ref. 18, the variation of the (bonding) interatomic distances and angles with composition is as shown in Fig. 5. This illustration is merely a more detailed version of information expressed in Fig. 1 of Ref. 18. The roughly parallel behaviour of the curves for X = As and X = Sb is conspicuous. The $T-X$ distances in $Cr_tFe_{1-t}X_2$ break this pattern, and the two crystallographically non-equivalent distances $d_1(\times 4)$ and $d_2(\times 2)$ become equal at $t \approx 0.5$ for X = As and $t \approx 1$ for X = Sb. As for the rest of the FeS_2-*m* type compounds, the condition $d_1 = d_2$ is only found (within standard deviations) for $CuSe_2$[6] and $OsSb_2$.[18] $Cr_tFe_{1-t}As_2$ is unique among the FeS_2-*m*

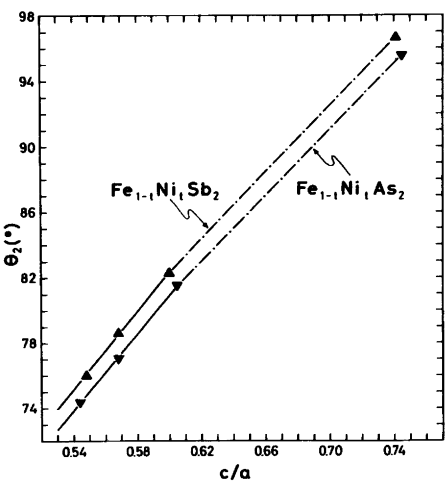

Fig. 6. Correspondence between one of the $T-X_6$ octahedral angles, θ_2, and axial ratio, c/a, for $Fe_{1-t}Ni_tX_2$.

type compounds in obeying the condition $d_1 < d_2$ (for $t > \sim 0.5$). Further knowledge is needed in order to correlate this with the instability (at least at temperatures ≥ 600 °C) of $Cr_tFe_{1-t}As_2$ for $t > 0.83$.

As also noted in Ref. 18 for binary FeS_2-*m* type compounds, the octahedral angle θ_1 (Fig. 5) is remarkably constant. Although the tetrahedral angles ϕ_1, ϕ_3 and ϕ_4 vary systematically with composition, the angle $\theta_2 = \phi_2$ (common to the $T-X_6$ octahedron and $X-T_3X$ tetrahedron) changes appreciably. The main variation of this angle is confined to the domain of $Fe_{1-t}Ni_tX_2$, *i.e.* in the transition region between classes A and B of the FeS_2-*m* type structure. In accord with this, there is a simple relationship between θ_2 and the axial ratio *c/a* (Fig. 6), which is in turn a consequence of the main features of the FeS_2-*m* type geometry.[19] The relation illustrated in Fig. 6 also shows that classification of the FeS_2-*m* type compounds according to axial ratios or θ_2 leads to essentially the same result. This aspect has been briefly discussed in Refs. 5 and 18.

(iii) Magnetic susceptibility data. The experimental $\chi_g^{-1}(T)$ curves (not corrected for induced diamagnetism) shown in Fig. 7 for $Cr_tFe_{1-t}As_2$ appear to fulfil Curie-Weiss law $[\chi^{-1} = C^{-1}(T-\theta)]$ at "low" temperatures. At "higher" temperatures the curves become concave towards the temperature axis. This tendency diminishes gradually with increasing t and disappears for $t \geq 0.6$ where the linearity in $\chi_g^{-1}(T)$ extends to the highest temperature of the measurements. The overall paramagnetic moment ($\mu_P = \sqrt{8C_{mol}}$) and the Weiss constant (θ) as derived from the (assumed, *vide infra*) Curie-Weiss law regions, are given on the inset of Fig. 7. The parameter μ_P is seen to increase in a roughly

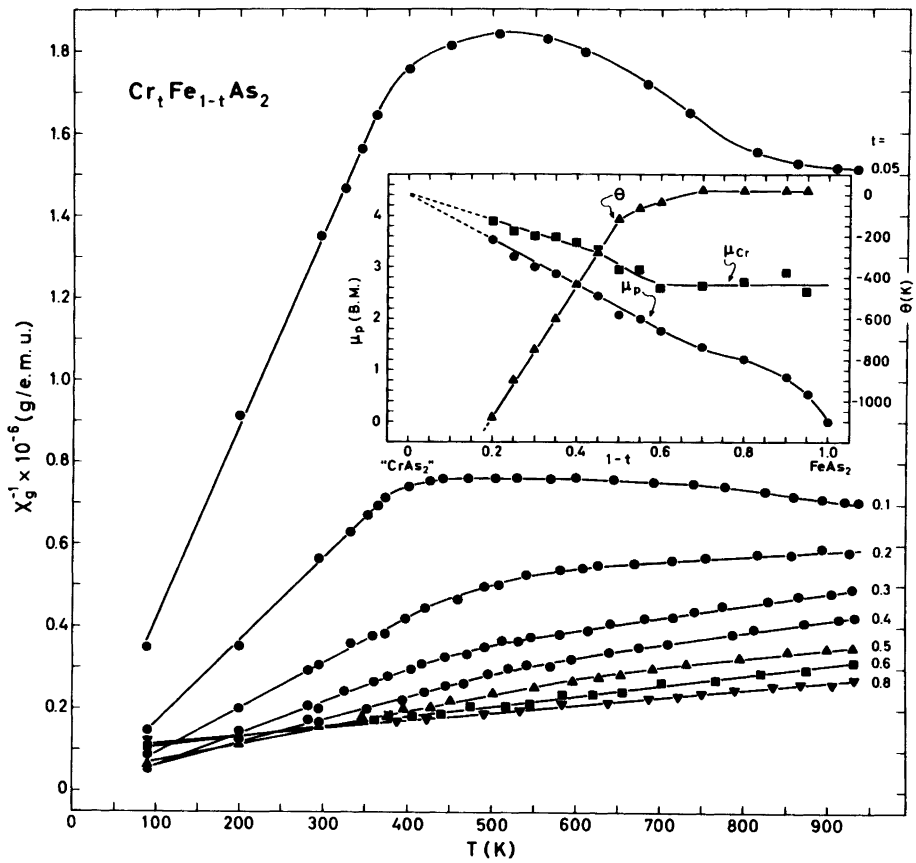

Fig. 7. $\chi_g^{-1}(T)$ curves for $Cr_tFe_{1-t}As_2$ (the diagram includes only about half of the experimental curves). Inset gives corresponding Curie-Weiss values of μ_P and θ. μ_{Cr} is estimated as outlined in the text.

linear manner from 0 ($t=0$) to 3.52 B.M. ($t=0.80$), whereas θ stays (within the uncertainty) constant at the zero value up to $t\approx 0.5$ and decreases thereafter approximately linearly from -120 ± 100 ($t=0.5$) to -1080 ± 100 K ($t=0.80$).

Although the above presentation follows the traditional pattern for evaluation of magnetic susceptibility data, it must be emphasized that association of the Curie-Weiss law with a linear section of a $\chi^{-1}(T)$ curve represents an unsettled assumption. At this stage it is natural to make another assumption on roughly the same level. Taking account of the facts that $FeAs_2$ is diamagnetic and that Cr carries two unpaired electrons in $CrSb_2$, Cr alone may be suspected to be responsible for the paramagnetic behaviour of $Cr_tFe_{1-t}As_2$. On this basis a Cr moment is derived according to $\mu_{Cr}=\mu_P\sqrt{t}$. As seen from Fig. 7, μ_{Cr} appears to stay approximately constant for $0<t<0.50$ (the comparatively large uncertainty in μ_{Cr} for small t being worth noting). In this concentration range μ_{Cr} complies with the "spin only" value, $\mu_{Cr}=2\sqrt{S(S+1)}$ B.M., for two unpaired electrons. For $t>0.50$ (when also θ becomes significantly different from zero) μ_{Cr} exceeds the "spin only" value.

Considerable effort has been devoted to the evaluation of the data in Fig. 7. The main problems associated with their interpretation appear to account for:

(1) The "too large values" of the magnetic moments.
(2) The large numerical values of θ.
(3) The shape of the $\chi^{-1}(T)$ curves and their variation with t.

A simple and traditional remedy to problem (1) is to allow for orbital contributions to the magnetic moment. Assuming that the essentially non-bonding, localized electrons on Cr in $Cr_tFe_{1-t}As_2$ may be referred to as a d^2 manifold, the spectroscopic ground term should be ^3F. Thus, with $S=1$ and $L=3$ a value of $\mu_{Cr}=[4S(S+1)+L(L+1)]^{\frac{1}{2}}$ B.M. $=4.47$ B.M. is obtained in terms of a weak $L-S$ coupling (narrow multiplet widths compared to kT) model. Accidental or not, it is interesting to note that this value of μ_{Cr} closely matches that obtained on extrapolating the curve in Fig. 7 to $t=1$. With such a starting point the statement "too large values" (which refers to the "spin only" situation) for μ_{Cr} no longer holds. In order to account for the decrease in μ_{Cr} with decreasing t, it is necessary to introduce a variable parameter for the degree of orbital quenching; complete quenching being the case for $t<0.5$. The puzzle is now shifted to that of accounting for a variable degree of orbital quenching. To achieve a more profound understanding it seems necessary to return to the fundamental concept of magnetic moment, *i.e.* its nature (creation, dissection in simpler constituents, *etc.*) and how it is influenced by the chemical bonding situation.

The behaviour of θ for $t>0.5$ (Fig. 7) suggests that $Cr_tFe_{1-t}As$ should adopt a cooperative magnetic mode over the relevant concentration range. This inference is, however, contrary to the results of the present neutron diffraction results (see *iv*), which show that $Cr_tFe_{1-t}As_2$ remains paramagnetic down to 10 K. Hence, these findings do not easily comply with the current apprehension of the relation between θ and the occurrence of cooperative magnetism.

To account for the shape of the $\chi^{-1}(T)$ curves in Fig. 7, it appears necessary to introduce the conception of electron excitations between states which are magnetically different. Such excitation processes would involve terms (one or more, depending on t) of the type $\exp(-\Delta/kT)$, where Δ represents the band gap energy. Omission of such temperature dependent terms occurs when $\Delta/kT\rightarrow\infty$ or $\Delta/kT\rightarrow 0$, *i.e.* at very low or very high temperatures compared to Δ/k. Again the problem is to put these findings into a broader reference frame.

The magnetic susceptibility data for $Cr_tFe_{1-t}As_2$ have released a number of interesting, apparently fundamental, but not yet understood questions. When these are added to the non-existence of cooperative magnetic phenomena and that $Cr_tFe_{1-t}As_2$ ceases to exist for $t>0.83$, it must be said that most properties of this phase are rather odd.

The magnetic susceptibility data for $CrSb_2$ have hitherto also belonged to the odd category. In view of the partial oxidation of $Cr_tFe_{1-t}Sb_2$ (which is not detected for $Cr_tFe_{1-t}As_2$, *vide supra*) it seemed likely that this peculiarity had a "natural" explanation. Hence, magnetic susceptibility measurements on $CrSb_2$ single crystals (made from chemical transport reactions and ground in an argon atmosphere) were performed. The results shown in Fig. 8 have removed the previously recorded anomalies (*cf.*, *e.g.*, Refs. 20 and 21). The Néel temperature (T_N) suggested from the shape of the curve in Fig. 8, agrees with the values obtained by neutron diffrac-

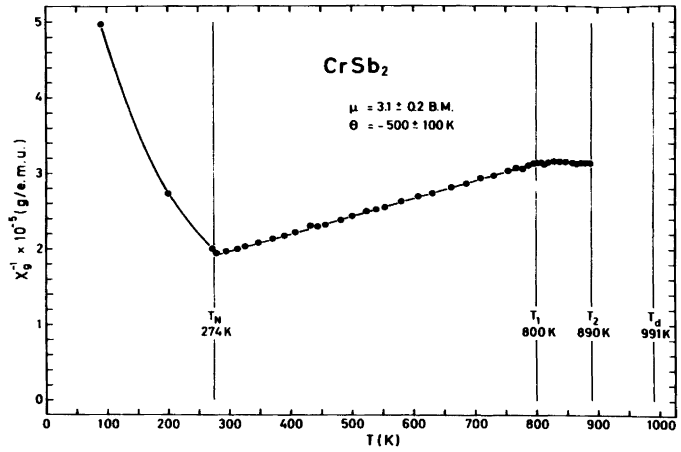

Fig. 8. Reciprocal magnetic susceptibility *versus* temperature for $CrSb_2$.

tion (273 ± 2 K, Ref. 1) and heat capacity measurements (274.1 K, Ref. 16). The paramagnetic moment of 3.1 ± 0.2 B.M. (derived from the Curie-Weiss region between T_N and $T_1=800$ K) is only slightly higher than the value expected for two unpaired electrons (see *iv*) from the "spin only" approximation. Decomposition according to $CrSb_2(s)\rightarrow$ $\sim$CrSb(s)+"Sb"(l) (as determined by DTA, high temperature X-ray diffraction, and quenching experiments with subsequent metallographic examinations) takes place at $T_d=991\pm3$ K (see also Ref. 16). However, the onset of oxidation and partial decomposition (*via* the gaseous phase) take place at a lower temperature. From supplementary experiments, it is found that oxidation of $CrSb_2$ varies with annealing time, silica quality, *etc.* The temperature $T_2=890$ K refers, therefore, to the first detectable oxidation of $CrSb_2$ under the experimental conditions during the magnetic susceptibility measurements. Cycled magnetic susceptibility measurements above T_2 produced (depending on annealing time) curves more and more similar to those published in Refs. 20 and 21. (Attempts to prepare single crystals of $Cr_tFe_{1-t}Sb_2$ with $t\neq0$ and 1 by chemical transport reactions have hitherto been unsuccessful.)

(iv) Cooperative magnetism. Neutron diffraction data for $Cr_tFe_{1-t}As_2$ ($t=0.63$ and 0.79), $Fe_{1-t}Ni_tAs_2$ ($t=0.50$) and $Fe_{1-t}Ni_tSb_2$ ($t=0.50$) collected at various temperatures between 10 and 293 K show no purely magnetic reflections, and any contributions of magnetic origin to the nuclear reflections must be very small. Any possible ordered moment in these phases is estimated to be less than 0.1 B.M. (max. limit covering all test models tried). The results exclude the possibility of a normal cooperative magnetic phenomenon occurring in $Cr_tFe_{1-t}As_2$, thus contributing to classification of its magnetic susceptibility data as anomalous (see *iii*).

Samples of $Cr_tFe_{1-t}Sb_2$ with $t=1$, 0.93, 0.88, 0.72, 0.60 and 0.45 were subjected to neutron diffraction examination between 10 and 293 K. The results show that the antiferromagnetic mode of $CrSb_2$ [1] extends to $t\approx0.5$ of the ternary $Cr_tFe_{1-t}Sb_2$ phase. The magnetic unit cell (a_M, b_M, c_M) of $Cr_tFe_{1-t}Sb_2$ is accordingly related to the chemical unit cell (a, b, c) by: $a_M=a$, $b_M=2b$, $c_M=2c$. The antiferromagnetic structure is of the simple uniaxial type. The phase relationships between the moments are such that these are coupled ferromagnetically within (011) of the chemical cell, the moments in adjacent planes being antiparallel. The free magnetic variables of this arrangement (see Fig. 1 of Ref. 1) are thus the components (μ_1, μ_2, μ_3) of the moment along a_M, b_M and c_M.

The magnetic parameters together with those specifying the chemical structure, thermal movements, and instrumental details were allowed as parallel variables in the profile refinement treatment of the neutron diffraction data. Although μ_2 was allowed as free variable in the initial refinements of each data set, this parameter was always found to be insignificantly different from zero and accord-

Table 2. Magnetic moment (μ_{tot}), its components (μ_1 and μ_3), Néel temperature (T_N) and deviation (δ) from the perpendicular to the diagonal plane (101) of the magnetic unit cell.

t	μ_1(B.M.)	μ_3(B.M.)	μ_{tot}(B.M.)	T_N(K)	δ(°)
1.00[a]	1.40(4)	1.34(6)	1.94(4)	273±2	−1.1(2.0)
0.93[a]	1.41(4)	1.28(7)	1.90(3)	246±2	0.4(2.0)
0.88[a]	1.38(4)	1.22(5)	1.84(3)	210±2	1.2(2.0)
0.72[b]	1.17(4)	1.01(7)	1.55(4)	127±3	2.0(2.0)
0.60[b]	0.86(7)	0.79(11)	1.17(5)	60±5	0.2(2.0)

[a] Moment values at 80 K. [b] Moment values at 10 K.

ingly fixed at zero in the final refinements. The final values for μ_1, μ_3 and μ_{tot} are listed in Table 2, the structural data being found in Table 1. Table 2 also includes values for T_N and the deviation of the moments from the direction specified by the perpendicular to the diagonal plane (101) of the magnetic unit cell. The latter information shows unequivocally that the moments are in fact (within standard deviations) perpendicular to the mentioned diagonal plane.

The temperature dependence of the integrated intensity of the magnetic (011) reflection for $t=0.93$, 0.88, 0.72 and 0.60 of $Cr_tFe_{1-t}Sb_2$ is shown in Fig. 9 (data for $t=1$ being given in Fig. 3 of Ref. 1). A scaled Brillouin type relationship for $S=1$ is indicated for each data set. The slightly systematic deviations between the points recorded for increasing temperatures are probably due to lack of thermal equilibrium rather than hysteresis effects.

In short, the results for $Cr_tFe_{1-t}Sb_2$ fit nicely in with those found for $CrSb_2$.[1] The question is now whether the new findings allow further progress with the interpretations.

The stability conditions corresponding to the cooperative magnetic mode of $CrSb_2$ (and $Cr_tFe_{1-t}Sb_2$) are

$$J_1>0;\ J_2<0;\ J_3<0;\ J_2J_3>{J_4}^2$$

as derived by application of the lattice theory of spin configurations.[1,22] The four exchange parameters J_1, J_2, J_3 and J_4 represent the interactions between nearest neighbour pairs of magnetic atoms along a, b, c and the body diagonals of the chemical unit cell, respectively.

The introduction of

$$|J_2| = |v|-\Delta$$
$$|J_3| = |v|+\Delta$$

gives

$$|J_2\|J_3| = J_2J_3 = v^2-\Delta^2,$$
$$v^2>v^2-\Delta^2 = J_2J_3>{J_4}^2$$

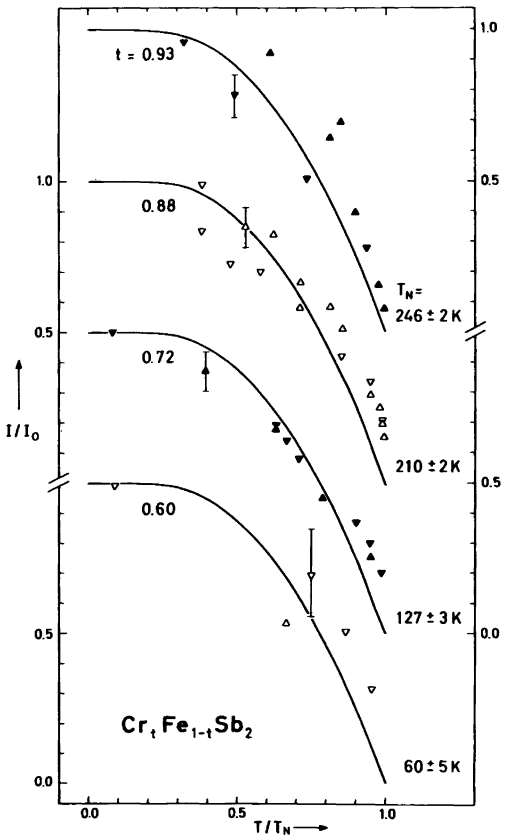

Fig. 9. Normalized, integrated intensity of the magnetic (011) reflection *versus* reduced temperature for $t=0.93$, 0.88, 0.72 and 0.60 of $Cr_tFe_{1-t}Sb_2$. Typical measurement errors are indicated. Symbols pointed upwards denote values obtained with increasing temperature, downwards with decreasing temperature. Curves show the Brillouin type relationship for $S=1$.

and hence

$$1/2(|J_2| + |J_3|) > |J_4|$$

T_N and θ can also be expressed in terms of the exchange parameters as:

$$T_N = \frac{2S(S+1)}{3k} \cdot \lambda, \quad \lambda = J_1 - J_2 - J_3$$

$$\theta = \frac{2S(S+1)}{3k} \cdot \lambda_F, \quad \lambda_F = J_1 + J_2 + J_3 + 4J_4$$

The observed T_N and θ for $CrSb_2$ give

$$\lambda + \lambda_F < 0$$

and since $J_1 > 0$, it follows that

$$J_4 < 0$$

The expressions for λ and λ_F can now be rearranged to

$$\lambda = J_1 + |J_2| + |J_3|$$
$$\lambda_F = J_1 - |J_2| - |J_3| - 4|J_4|$$

According to the experimental data for $CrSb_2$

$$2\lambda \approx -\lambda_F$$

and therefore

$$|J_4| \approx 1/4(3J_1 + |J_2| + |J_3|)$$

which gives rise to the two additional inequalities

$$J_1 < 1/3(|J_2| + |J_3|)$$

and

$$|J_4| > 1/4(|J_2| + |J_3|)$$

In order to proceed further with the interpretations along this line, data over and above those available at present are needed.

Two closely related questions naturally arise in relation to the variations of μ_{tot} ($=2\bar{S}$)* and T_N when $t \neq 1$ in $Cr_tFe_{1-t}Sb_2$ (Fig. 10):

(1) Does Fe carry an ordered magnetic moment?

(2) How are the magnetic exchange interactions communicated?

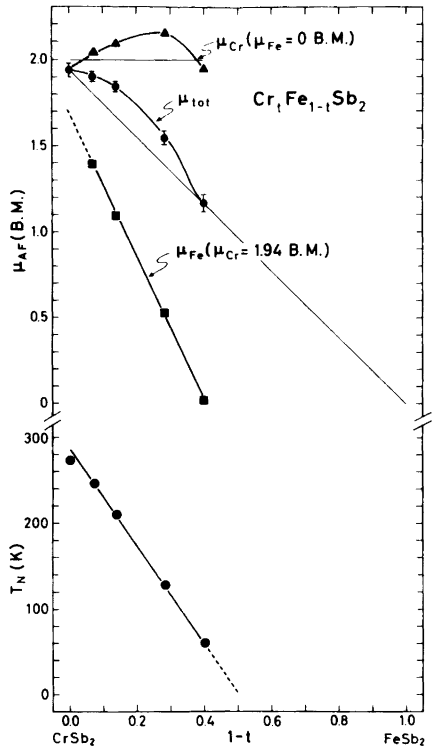

Fig. 10. Magnetic moment (μ_{tot}) and Néel temperature (T_N) as functions of t in $Cr_tFe_{1-t}Sb_2$. μ_{Fe} indicates the Fe contribution to μ_{tot} based on $\mu_{Cr} = 1.94$ B.M. = const.; μ_{Cr} the Cr contribution when $\mu_{Fe} = 0$ B.M. = const. Error bars on μ_{tot} correspond to the calculated standard deviations in Table 3.

If the answer to question (1) is yes, the next concern will be the size of the Fe contribution. The observed magnetic moment (μ_{tot}) may be split in contributions from Cr and Fe according to

$$\mu_{tot} = t\mu_{Cr} + (1-t)\mu_{Fe}$$

In order to proceed further, additional assumptions must be made. Tentatively it is natural to look at two simple situations, either (a) $\mu_{Cr} = 1.94$ B.M. or (b) $\mu_{Fe} = 0$ B.M. constant, independent of t (*viz.*

* The symbol μ is used in a somewhat different sense in section *iii.*

$t \neq 1$). The results of these evaluations are depicted in Fig. 10. Situation (a) is seen to demand substantial variation of μ_{Fe} (burdened with large errors) with t, whereas (b) leads to a fairly concentration independent Cr contribution ($\mu_{Cr} \approx 2$ B.M. when reasonable uncertainties are allowed for). Both results are physically conceivable, and in order to make a choice, information on other properties must be taken into account.

Mössbauer spectroscopy appears as a convenient tool to attack problems of this type. Bargeron *et al.*[23] have, for example, substituted (up to) 2 % ^{57}Fe into samples of MnS_2, $MnSe_2$ and $MnTe_2$ and shown that at atmospheric pressure the resulting Mössbauer parameters are characteristic of high spin Fe(II). They furthermore showed that the high spin situation can be converted to low spin by squeezing the atoms together under the application of high pressure. The inference from their findings is that there is a definite correspondence between the Fe–X bond length and the Fe spin state as reflected by the Mössbauer parameters, in particular the quadrupole splitting parameter (Δ).

Fig. 11 shows the correlation between Δ and the average T–X bond length for the series FeP_2 – $FeAs_2$ – $FeSb_2$ – $Cr_tFe_{1-t}Sb_2$ together with data for $Cr_tFe_{1-t}As_2$. This illustration, which invites to extension to other related compounds and phases, could call for a comprehensive discussion. However, we shall here stick to the subject and only make two quite simple derivations:

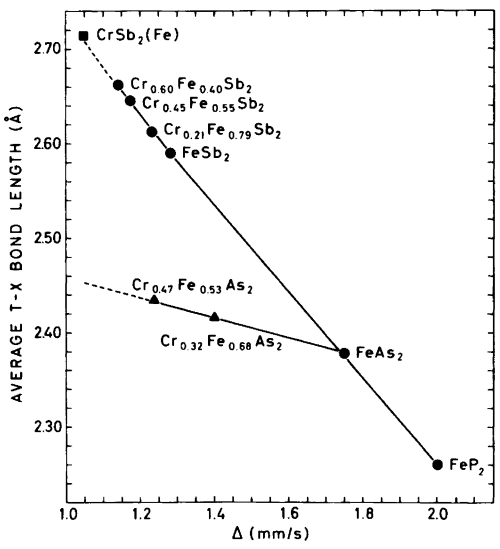

Fig. 11. Average T–X bond length *versus* quadrupole splitting parameter Δ. (Data not included in this paper are taken from Refs. 2, 24 and 25.)

(1) The electron configuration associated with Fe in $Cr_tFe_{1-t}Sb_2$ is essentially the same as in FeP_2, $FeAs_2$ and $FeSb_2$. Hence, as the latter compounds consist of spin-paired Fe this must also be the case for $Cr_tFe_{1-t}Sb_2$. From the virtually linear correlation in Fig. 11 it seems very unlikely that the Fe atoms in $Cr_tFe_{1-t}Sb_2$ carry any magnetic moment.

(2) Once again the anomalous character of $Cr_tFe_{1-t}As_2$ is being emphasized.

The relationship between the Mössbauer parameters and the structural features of these phases will be taken up in a broader context in a forthcoming paper.

Accepting that Fe carries no magnetic moment, the question of how the exchange interactions are communicated in $Cr_tFe_{1-t}Sb_2$ may be put on an equal footing to the corresponding questions concerning, *e.g.*, the many solid solution oxide phases considered by Goodenough.[26] The time appears not quite ready for a fruitful approach to this comprehensive problem. However, one brief, phenomenalistic comment concerning $Cr_tFe_{1-t}Sb_2$ should be made. Fig. 10 shows that the Néel temperature follows the (approximate) empirical relation

$$T_N = T_{N,CrSb_2}(2t-1)$$

A simple dilution model on statistical basis would suggest that

$$T_N = T_{N,CrSb_2}[\alpha t^2 + \beta 2t(1-t) + \gamma(1-t)^2]$$

where α, β and γ are weight functions for local exchange terms representing Cr–Cr, Cr–Fe and Fe–Fe nearest neighbour communicators, respectively. According to the empirical relation and given $\alpha = 1$, it follows that $\beta \approx 0$ and $\gamma \approx -1$. This implies that two (or more) consecutive Fe are destructive to the magnetic mode whereas the single Fe atoms act as neutral "diluters".

Acknowledgement. This work has received financial support from The Norwegian Research Council for Science and the Humanities.

REFERENCES

1. Holseth, H., Kjekshus, A. and Andresen, A. F. *Acta Chem. Scand. 24* (1970) 3309.
2. Kjekshus, A. and Rakke, T. *Acta Chem. Scand. A 28* (1974) 1001.
3. Kjekshus, A. and Rakke, T. *Unpublished results.*
4. Jeitschko, W. and Donohue, P. C. *Acta Crystallogr. B 29* (1973) 783.
5. Kjekshus, A. and Rakke, T. *Acta Chem. Scand. A 31* (1977) 517.
6. Kjekshus, A., Rakke, T. and Andresen, A. F. *Acta Chem. Scand. A 28* (1974) 996.
7. Holseth, H. and Kjekshus, A. *Acta Chem. Scand. 23* (1969) 3043.
8. Roseboom, E. H. *Am. Mineral. 48* (1963) 271.
9. Bjerkelund, E. and Kjekshus, A. *Acta Chem. Scand. 24* (1970) 3317.
10. Holseth, H. and Kjekshus, A. *Acta Chem. Scand. 22* (1968) 3273.
11. *The 1976-compilation of the Neutron Diffraction Commission.*
12. Rietveld, H. M. *J. Appl. Crystallogr. 2* (1969) 65.
13. Hulliger, F. *Nature (London) 198* (1963) 1081.
14. Holseth, H. and Kjekshus, A. *Acta Chem. Scand. 22* (1968) 3273.
15. Haraldsen, H., Rosenqvist, T. and Grønvold, F. *Arch. Math. Naturvidensk. 50* (1948), No. 4.
16. Alles, A., Falk, B., Westrum, E. F. and Grønvold, F. *J. Chem. Thermodyn. 10* (1978) 103.
17. Brostigen, G., Kjekshus, A. and Rømming, C. *Acta Chem. Scand. 27* (1973) 2791.
18. Kjekshus, A., Rakke, T. and Andresen, A. F. *Acta Chem. Scand. A 31* (1977) 253.
19. Kjekshus, A. and Rakke, T. *To be published.*
20. Holseth, H. and Kjekshus, A. *J. Less-Common Met. 16* (1968) 472.
21. Adachi, K., Sato, K. and Matsuura, M. *J. Phys. Soc. Jpn. 26* (1969) 906.
22. Bertaut, E. F. In Rado, G. T. and Suhl, H., Eds., *Magnetism III*, Academic, New York – London 1963, Chapter 4.
23. Bargeron, C. B., Avinor, M. and Drickamer, H. G. *Inorg. Chem. 10* (1971) 1338.
24. Dahl, E. *Acta Chem. Scand. 23* (1969) 2677.
25. Kjekshus, A. and Nicholson, D. G. *Acta Chem. Scand. 25* (1971) 866.
26. Goodenough, G. B. *Magnetism and the Chemical Bond*, Interscience, New York – London 1963.

Received January 17, 1979.